JACS
JOURNAL OF THE AMERICAN CHEMICAL SOCIETY

Article

pubs.acs.org/JACS

Concerted Amidation of Activated Esters: Reaction Path and Origins of Selectivity in the Kinetic Resolution of Cyclic Amines via N-Heterocyclic Carbenes and Hydroxamic Acid Cocatalyzed Acyl Transfer

Scott E. Allen,[†] Sheng-Ying Hsieh,[‡] Osvaldo Gutierrez,[†] Jeffrey W. Bode,*[,‡] and Marisa C. Kozlowski*[,†]

[†]Department of Chemistry, Roy and Diana Vagelos Laboratories, University of Pennsylvania, Philadelphia, Pennsylvania 19104, United States

[‡]Laboratorium für Organische Chemie, ETH-Zürich, Zürich 8093, Switzerland

Supporting Information

ABSTRACT: The N-heterocyclic carbene and hydroxamic acid cocatalyzed kinetic resolution of cyclic amines generates enantioenriched amines and amides with selectivity factors up to 127. In this report, a quantum mechanical study of the reaction mechanism indicates that the selectivity-determining aminolysis step occurs via a novel concerted pathway in which the hydroxamic acid plays a key role in directing proton transfer from the incoming amine. This modality was found to be general in amide bond formation from a number of activated esters including those generated from HOBt and HOAt, reagents that are broadly used in peptide coupling. For the kinetic resolution, the proposed model accurately predicts the faster reacting enantiomer. A breakdown of the steric and electronic control elements shows that a gearing effect in the transition state is responsible for the observed selectivity.

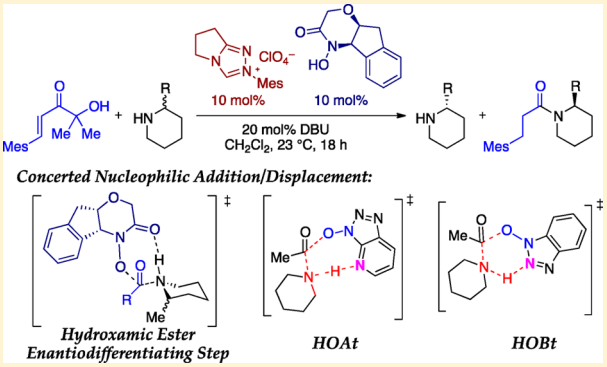

INTRODUCTION

Kinetic resolution is a valuable tool for the synthesis of enantiopure materials from racemic mixtures.[1] Typically, these reactions entail the rapid reaction of one enantiomer of a racemate with a chiral catalyst, which allows for the isolation of enantioenriched unreacted starting material as well as an enantioenriched product. Many compounds that act as acyl transfer regents for kinetic resolution have been reported, including 4-aminopyridines, *N*-alkylimidazoles, amidines, and N-heterocyclic carbenes (NHCs).[2] In a typical reaction, the chiral nucleophilic transfer reagent is acylated by a carboxylic acid derivative. This moiety activates the acyl group for preferential nucleophilic displacement by one enantiomer of the substrate, releasing the chiral catalyst.

The origins of selectivity for the kinetic resolution of secondary alcohols involving acyl transfer as catalyzed by 4-aminopyridine analogues,[3] amidines,[4] tetrapeptides,[5] and yttrium salen complexes[6] have been elucidated via experiment and computation. Cation-π effects have been found to govern the acyl transfer-mediated kinetic resolution of lactams and thiolactams with amidine catalysts.[7] Despite the widespread importance of amine acylation reactions, the precise details of the mechanism of the kinetic resolution of unactivated amines have never been fully elucidated, reflecting a fundamental gap in the literature.

In 2011, the Bode lab reported a kinetic resolution of 2-substituted cyclic amines using a dual catalyst system consisting of an achiral NHC **3** and a chiral hydroxamide **4** (eq 1).[8] This process offered the first catalytic method for resolving enantiomers of chiral N-heterocycles including piperazines, piperidines, morpholines, and isoquinolines.[9]

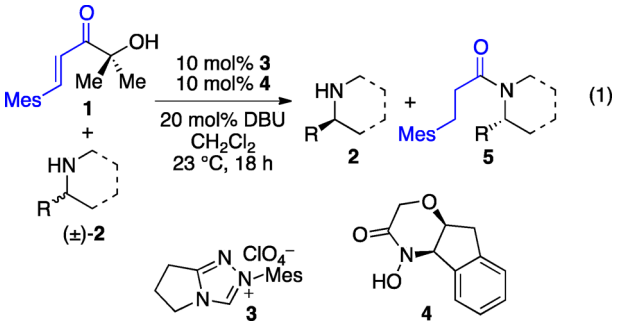

When the resolution reaction is performed in the absence of amine, chiral hydroxymate ester **7** is formed by the NHC-catalyzed acylation of **4** with **1**. This ester is stable and can be isolated by column chromatography. Treatment of ester **7** with

Received: June 9, 2014
Published: July 22, 2014

   dx.doi.org/10.1021/ja505784w | J. Am. Chem. Soc. 2014, 136, 11783−11791

2-methylpiperidine affects the kinetic resolution with the same selectivity as the catalytic method in eq 1 (Scheme 1).[10] In

Scheme 1. Effect of Ester Structure on Selectivity Factor

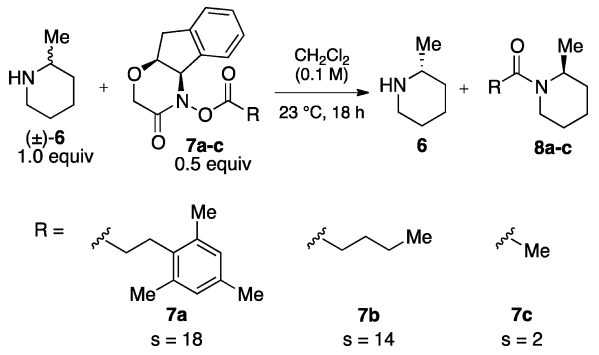

addition, solid supported versions of **4** are highly effective in kinetic resolution of amines.[8c] These observations suggest that the only chemical species necessary for the key resolution step are the hydroxamic ester and the amine.

In this paper, density functional theory (DFT) calculations support a reactivity enhancement in the amine acylation due to hydrogen bonding of the incoming amine nucleophile by the carbonyl of the hydroxamic acid moiety. Computations with other commonly used acyl transfer reagents (HOBt, HOAt, and 7-Cl-HOBt) also show a strong preference for this bimolecular mechanism via a concerted 6/7-member transition state. The mechanism also accounts for the results observed with highly and poorly selective substrates. Implications for the rational design of novel acyl transfer reagents are discussed.

RESULTS AND DISCUSSION

Paramount to understanding the origin of the reactivity and selectivity in a kinetic resolution proceeding through an aminolysis mechanism (Scheme 1) is elucidation of the reaction pathway. Although introductory organic texts propose a mechanism in which the amine adds to the ester to generate a zwitterionic intermediate,[11] theoretical studies indicate that this intermediate is high in energy and can be located only through the inclusion of at least five explicit water molecules.[12] This arrangement is possible in aqueous solution[13] but is unlikely in dry organic solvents. The zwitterionic pathway can also be promoted by 2-pyridinone[14] and within enzymatic active sites.[15]

The formation of amides from esters is a key reaction in synthesis, and studies to date have shown that the transformation proceeds through a neutral transition state in which nucleophilic addition and displacement accompanies proton transfer.[16−19] In a two-step pathway (Scheme 2), the amine undergoes nucleophilic attack with concurrent proton transfer via **9A-TS1** to generate a tetrahedral intermediate (**9B**). The alcohol nucleofuge departs in a second, neutral step (**9A-TS2**). In a potential concerted mechanism, addition and elimination occur simultaneously, without explicit participation of the carbonyl via **9A-TS**.

A proton transfer catalyst, such as water, can promote both reaction pathways (Scheme 3).[17,18] The water-mediated proton transfer alleviates the strain associated with a four-membered proton transfer.[20,21] This role can also be served by a vicinal alcohol.[22,23] A second amine molecule can also facilitate the proton transfer via the general base pathway.[24−27] Theoretical[19]

Scheme 2. Uncatalyzed Aminolysis Pathways

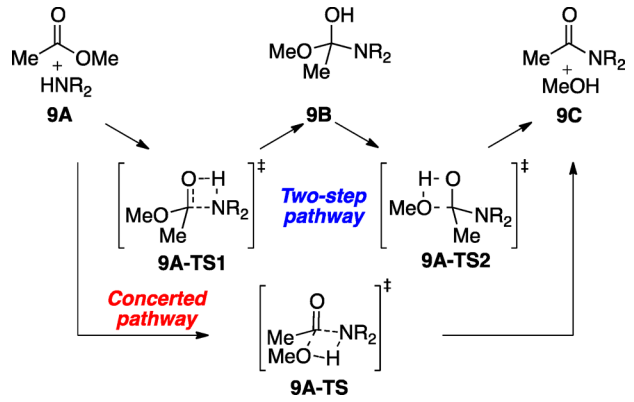

Scheme 3. Aminolysis Pathways with Water-Catalyzed Proton Transfer

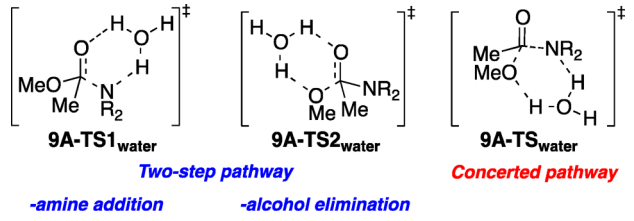

and experimental[28] studies have shown that 2-pyridinone, acetic acid,[29] and triazabicyclodecene (TBD)[30] can also act as proton conduits. In many systems, the two-step and concerted pathways are nearly isoelectronic; greater differentiation comes from steric and electronic interactions between the reacting partners.

Kinetic studies of the reaction in Scheme 1 indicated that the reaction is first order in amine;[31] therefore, the general base pathway, in which a second equivalent of amine facilitates the proton transfer, was not explored. For the elementary reaction path studies, a model system utilizing methyl acetate (Scheme 1, R = Me) and unsubstituted piperidine were employed in order to minimize the conformational freedom in the transition state. Both the water-catalyzed (hydrous) and uncatalyzed (anhydrous) pathways were examined.

The differences between the solvated and gas-phase relative free energies (Figure 1) show the importance of implicit solvation in modeling these reaction pathways due to the large amount of charge separation. The black lines represent the anhydrous reaction path, while the blue lines indicate the hydrous path. The inclusion of water as a proton transfer agent lowers the energy of activation in the first step of the two-step pathway (Figure 1, **10A-TS1** vs **10A-TS1**$_{water}$) by ca. 7 kcal/mol. The presence of water in this transition state allows for an N−H−O angle of 153°, as opposed to 112° in the anhydrous reaction. In the anhydrous transition state, the N−H bond must lie parallel to the carbonyl for optimum proton transfer, inducing significant strain between the substitution on the carbonyl and C2 and C6 of the piperidine ring. This strain is alleviated slightly in the hydrous transition state.

For the two-step pathways, the transition state between the two tetrahedral intermediate rotamers (**10-B** and **10-B**$_{conf}$) from the first and second steps was not located; presumably, the barrier to interconversion of these rotamers will be much smaller than the other barriers. The second step, elimination of the hydroxamide, does not benefit from the inclusion of an

dx.doi.org/10.1021/ja505784w | J. Am. Chem. Soc. 2014, 136, 11783−11791

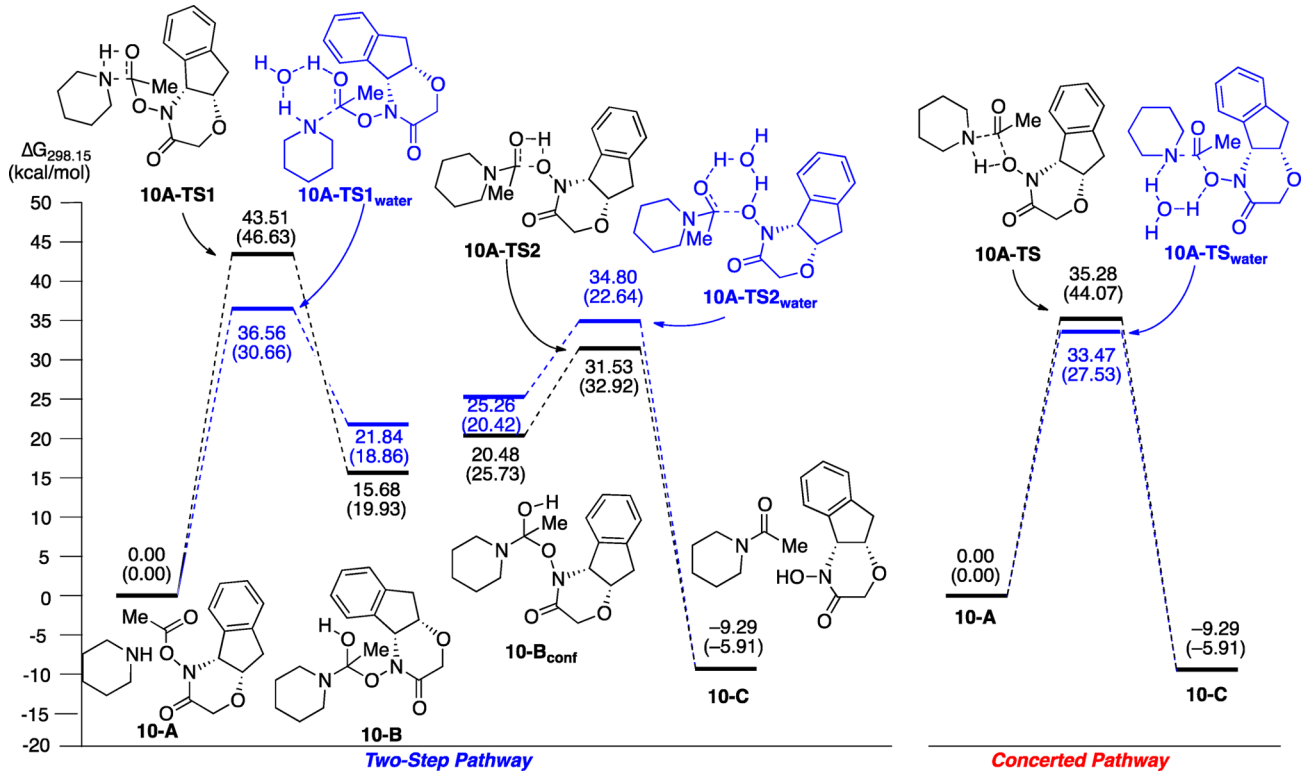

Figure 1. Reaction coordinate for the hydrous (blue) and anhydrous (black) two-step pathway (left) and concerted pathway (right). Relative Gibbs free energy values calculated at IEPCM-CH_2Cl_2-M06-2X/6-311+G(d,p)//B3LYP/6-31G(d,p);[32] parenthetical values are gas-phase B3LYP/6-31G(d,p) free energies.

explicit water molecule (**10A-TS2** vs **10A-TS2**$_{water}$). Here, the entropic cost of the trapped water molecule is not sufficiently compensated by the enthalphic benefits of the larger angles of proton transfer.[31] The second step of the hydrous two-step mechanism lies less than 2 kcal/mol lower than the first step, suggesting that the rate-limiting step may vary given the substitution in the system. On the other hand, the elimination step (**10A-TS2**) of the anhydrous pathway is over 10 kcal/mol lower in energy than the addition step (**10A-TS1**). The anhydrous proton transfer still proceeds at an unfavorable angle, but the steric strain between the carbonyl and the departing hydroxamide is significantly lower compared to the approach of the secondary amine in the first step.

In the concerted path (Figure 1, right), the nucleophilic attack of the piperidine occurs with simultaneous proton transfer and departure of the hydroxamide via **10A-TS**/**10A-TS**$_{water}$. The amine approach necessary for this reaction alleviates much of the steric strain observed in the first step of the two-step pathway. The wider proton transfer angle of the hydrous transition state **10A-TS**$_{water}$ lowers the energy of activation for this pathway, but only by 1.81 kcal/mol. Notably, the lowest energy conformation of the hydrous concerted pathway is 3.09 kcal/mol lower in energy than the rate-determining first step of the hydrous two-step pathway.

Since the barriers of all the above processes were high relative to the experimental barrier (~22 kcal/mol based on observed reaction rates and times),[8a] a third mechanism was investigated. In this variant of the concerted mechanism, the carbonyl of the hydroxamide removes the proton from the amine as the leaving group departs (Figure 2). Notably, a related six-membered transition state was found not to be the operative pathway in ester amination under pyridone catalysis

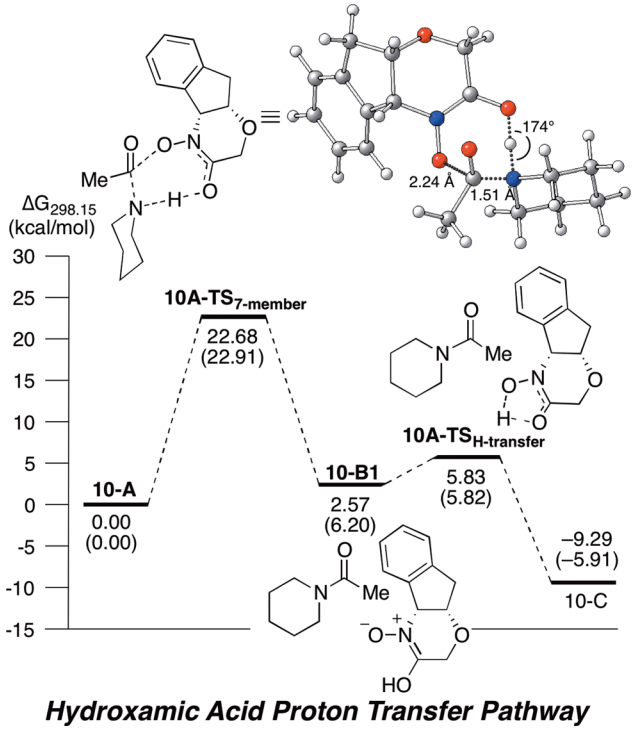

Figure 2. Reaction coordinate for the seven-membered concerted transition state pathway at the IEPCM-CH_2Cl_2-M06-2X/6-311+G(d,p)//B3LYP/6-31G(d,p); parenthetical values are gas-phase B3LYP/6-31G(d,p) free energies.

as reported by Wang and Zipse.[19] The lowest energy conformation of the seven-membered transition state (**10A-**

dx.doi.org/10.1021/ja505784w | J. Am. Chem. Soc. 2014, 136, 11783–11791

Table 1. Relative Reaction Barriers[a] for the Competing Pathways Using Representative Acyl Transfer Agents (4, 11−14) with Acetyl and Piperidine

transition state \ acylating agent	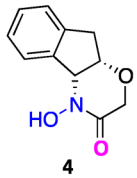 4	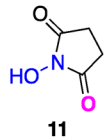 11	HOAt  12	HOBt 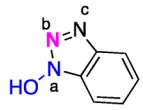 13	6-Cl-HOBt 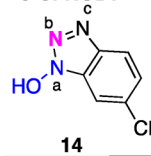 14
step-anhy-TS 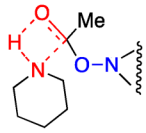	43.5	45.3	43.0	43.0	42.5
step-hyd-TS 	36.6	37.3	35.4	35.2	34.7
conc-anhy-TS 	35.3	27.0	22.5	23.0	22.0
conc-hyd-TS 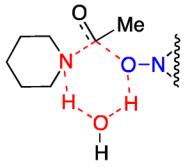	33.5	33.4	26.4	28.1	27.1
conc-$TS_{7\text{-member}}$ 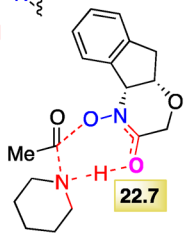 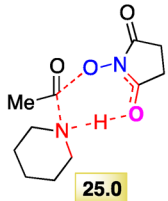 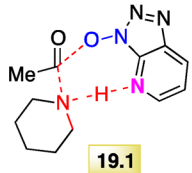	22.7	25.0	19.1	NA	NA
conc-$TS_{6\text{-member}}$ 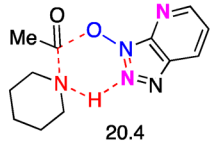 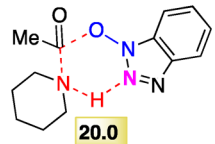 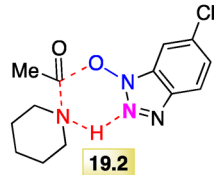	NA	NA	20.4	20.0	19.2

[a]Free energies in kcal/mol; IEPCM-CH_2Cl_2-M06-2X/6-311+G(d,p)//B3LYP/6-31G(d,p).

$TS_{7\text{-member}}$) is 10.79 kcal/mol lower in energy than the hydrous concerted transition state in (**10A-TS_{water}**; Figure 1). The subsequent proton transfer (**10A-$TS_{H\text{-transfer}}$**) that effects tautomerization of the nitrone to regenerate the hydroxamate cocatalyst, calculated here as an intramolecular process, requires little energy. On the basis of the much lower energy barriers for the intramolecular proton transfer (Figure 2 vs Figure 1), this pathway was utilized for the study of the enantioselective kinetic resolution process (see below). In comparison to the pathways discussed earlier (Figure 1), implicit solvation (see parenthetic values in the figures) has little effect on the activation energies for this reaction pathway (Figure 2).

To probe the generality of the concerted bimolecular reaction pathway involving C−N bond forming, C−O bond breaking, and concomitant proton transfer, we investigated the competing pathways for various commonly used acyl transfer reagents including *N*-hydroxysuccinimide (**11**), HOAt (**12**), HOBt (**13**), and 6-Cl-HOBt (**14**). In the reaction of the acetyl derivatives of **11**−**14** with piperidine, the lowest energy pathway for each (Table 1) involves concerted bond breaking/forming with concomitant proton transfer via either a seven-member transition state (**conc-$TS_{7\text{-member}}$**) or a six-member transition state (**conc-$TS_{6\text{-member}}$**). For HOAt, which can adapt either six- or seven-member TS with nitrogen N_b or nitrogen N_d, respectively, the seven-member transition state is slightly favored. Previous work has shown the importance of N_d in comparison to agents lacking this nitrogen [i.e., HOBt (**13**)[33] and variants of HOAt[34]] in the efficiency of peptide couplings, but no computational support, to date, has been reported.

These data convincingly show that a concerted addition/elimination mechanism involving proton transfer in a cyclic transition state plays a key role in amide bond formation with these broadly used reagents. This stands in contrast to mechanisms typically invoked involving stepwise addition/elimination and a tetrahedral intermediate. The stabilization of the concerted transition states arises from appropriate orientations of heteroatoms to facilitate a strain-free deprotonation of the incoming amine while forming the C−N bond (Figure 3). In particular, near ideal trajectories can be found in the seven-membered transition states of both hydroxamate **4** and HOAt (**12**) as evidenced by the O−H−N bond angles of 174° (Figure 2) and 169° (Figure 3), respectively. For HOAt, a direct comparison of the six- and seven-membered transition states (Figure 3) is possible and reveals that the former also facilitates a near ideal deprotonation (bond angle 174°) but at

dx.doi.org/10.1021/ja505784w | J. Am. Chem. Soc. 2014, 136, 11783−11791

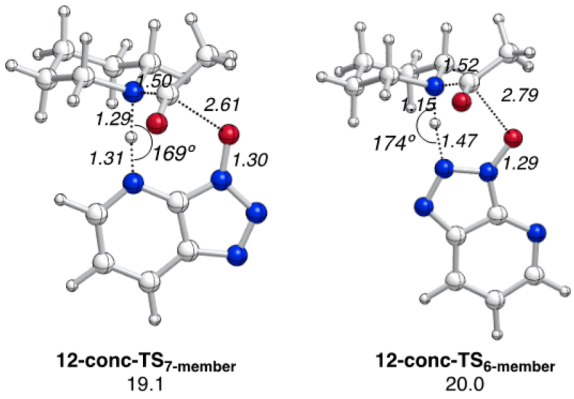

Figure 3. Structrures of the six- and seven-membered concerted transition state with HOAt (12) at IEPCM-CH_2Cl_2-M06-2X/6-311+G(d,p)//B3LYP/6-31G(d,p); bond distances indicated in Å, angles in degrees.

an energetic cost of 1 kcal/mol in accord with the slower rates observed with HOBt (**13**).[33]

The calculations also show that the overall barriers for acyl transfer reagents **12**−**14** are significantly lower than that for **4** leading to the expectation of faster rates with **12**−**14**. In accord with the computational data, kinetic studies (eq 2) show relative rates of **12** > **14** ≫ **4** in amide-forming reactions.

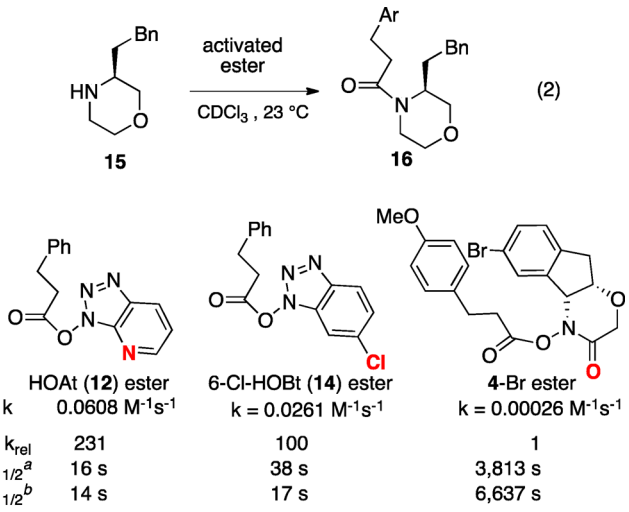

[a]From k with 1 M. [b]From ΔG‡ with 1 M.

With a likely reaction pathway in hand, our attention turned to the factors controlling the enantioselective acylation. In the stoichiometric resolution process, the pentanoate (**7b**, R = *n*-butyl, Scheme 1) gives very similar selectivity to the mesityl-substituted ester **7a**, suggesting that the aryl ring (and any electronic/dispersion interactions that accompany it) is not required for selectivity. However, the poor performance of the acetate (**7c**, R = Me) confirms that the ester cannot be completely truncated. In order to model the butyl group while minimizing the number of rotamers, the hydroxamic propionate (**7**, R = Et) was utilized. In addition, 2-methylpiperidine, which has well-defined conformations, was employed. In order to affirm the validity of this model, transition states and the selectivity factor were also obtained for the corresponding acetate (**7c**, R = Me, Scheme 1).

Examination of the seven-membered transition state reveals seven key variables that contribute to the conformational flexibility of this system. Through a systematic study of these variables with both enantiomers of 2-methylpiperidine, all of the 128 possible transition states were studied. The lowest energy ethyl rotamer for each possible combination is shown in the Supporting Information.[31] For these transitions states, the enthalpies[35] contributing to the Boltzmann distribution at 25 °C are tabulated in Table 2.[31] This table clearly depicts that the most stable transition state is similar for both the acetate and propionate substrates. Furthermore, the 10 lowest energy transition states account for the vast majority (~98%) of the product, but a significant redistribution of energies with R = Et explains the higher selectivity for the propionate.

Table 2. Relative Enthalpies (kcal/mol) and Boltzman Distribution for the Acetyl and Propionyl Derived Transition States Corresponding to Figure 5 in the Solvated Phase

		7 (R = Et)		7 (R = Me)	
TS	piperidine config	rel $\Delta H^{\ddagger a}$	(%)	rel $\Delta H^{\ddagger a}$	(%)
TS4	*S*	0.00	89.8	0.00	36.7
TS52	*S*	3.21	0.4	0.07	32.6
TS34	*R*	2.33	1.8	0.50	15.7
TS42	*R*	3.71	0.2	1.20	4.8
TS26	*R*	3.89	0.1	1.65	2.3
TS18	*R*	2.19	2.2	1.71	2.1
TS51	*S*	5.46	<0.1	2.08	1.1
TS8	*S*	2.37	1.7	2.27	0.8
TS1	*R*	2.31	1.8	2.45	0.6
TS38	*R*	4.29	0.1	2.57	0.5
TS6	*R*	2.80	0.8	2.65	0.4
TS33	*R*	4.21	0.1	2.68	0.4
TS12	*S*	2.98	0.6	2.89	0.3
TS56	*S*	4.37	0.1	2.89	0.3
TS60	*S*	5.05	<0.1	3.01	0.2
TS54	*R*	5.15	<0.1	3.16	0.2
TS41	*R*	8.01	<0.1	3.21	0.2
TS22	*R*	4.66	<0.1	3.39	0.1
TS2	*R*	3.74	0.2	3.43	0.1
TS30	*R*	7.17	<0.1	3.50	0.1
TS40	*S*	4.79	<0.1	3.51	0.1
TS27	*S*	4.89	<0.1	3.59	0.1
TS19	*S*	4.88	<0.1	3.76	0.1
TS46	*R*	5.57	<0.1	3.77	0.1
TS53	*R*	7.10	<0.1	3.85	0.1
TS7	*S*	4.05	0.1	4.01	<0.1

[a]All values calculated at 298 K using IEFPCM-CH_2Cl_2-M062X/6-311+G(d,p)//B3LYP/6-31G(d,p). For structural descriptions of each transition sate, see the Supporting Information.

The lowest energy transition state overall is depicted in the top left of Figure 4 (**TS4**). The energetic consequence of each conformational variable was assessed via comparison to this transition state. Most of the lowest energy transition states contained the (*S*)-enantiomer of 2-methylpiperidine. However, several transition states with (*R*)-enantiomer (e.g., **TS18**) do contribute significantly to the reaction outcome (within 2.5 kcal/mol of the lowest energy transition state).

The hydroxamic ester can undergo *cis-trans* isomerization (**TS36**$_{rot}$, Figure 4); in the absence of amine the *trans* conformation is 3 kcal/mol higher in energy. In the presence of amine, the *trans* conformation is even higher in energy because the conformational changes required to avoid the

dx.doi.org/10.1021/ja505784w | J. Am. Chem. Soc. 2014, 136, 11783−11791

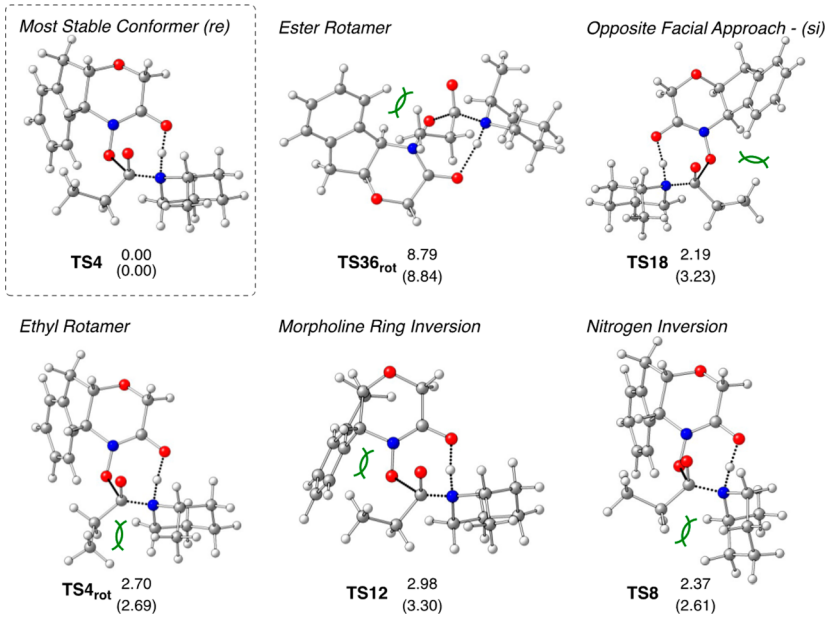

Figure 4. Lowest energy transition state and key steric interactions for each conformational variable. Relative enthalpies of activation (298 K, kcal/mol) from IEFPCM-CH_2Cl_2-M06-2X/6-311+G(d,p)//B3LYP/6-31G(d,p). Parenthetical values are the corresponding gas phase B3LYP/6-31G(d,p) values.

strong $A^{1,2}$ strain between the hydroxamide and the ester block the approach of the amine.

The chiral, nonracemic ester effects energetic differentiation of the *si*- and *re*-faces of the carbonyl group. In both approaches, the indane is directed away from the amine so that the hydroxamic acid carbonyl can remove the amine proton. In the more favored *re*-approach, the indane is directed away from the ethyl group. In the *si*-approach (**TS18**, Figure 4, top right), the indane abuts the ethyl group, causing an unfavorable steric interaction that renders all *si*-approaches higher in energy relative to their *re*-face counterparts. The lowest energy *si*-face transition state depicted (**TS18**) is also the lowest energy transition state for the more slowly reacting (*R*)-amine enantiomer.

The ethyl group of the hydroxamic acid propionate (Scheme 1, R = Et) has, in theory, three rotamers. In practice, however, one conformation is not viable due to steric overlap, and a second is routinely higher in energy (Figure 4, **TS4** vs $\mathbf{TS4_{rot}}$). In the higher energy conformation, the pendant methyl group orients toward the 2-methylpiperidine (Figure 5, top), imparting significant steric strain, while in the lower energy rotamer the methyl group nearly eclipses the carbonyl (Figure 5, bottom).

Ring inversion of the morpholine portion changes the orientation of the indane portion of the cocatalyst. When the morpholine oxygen lies *trans* to the indane (Figure 4, **TS12**), a destabilizing syn-pentane interaction is introduced between the *N*-hydroxyl group and the aromatic ring of the indane.

In the 2-methylpiperidine ring, nitrogen inversion occurs independently of ring inversion; the barrier to nitrogen inversion in piperidine is 6.1 kcal/mol.[36] Theoretical and experimental studies of 2-alkylpiperidine conformations have shown that the lowest energy conformation possesses an axial lone pair and equatorial substitution at the 2-position.[37] However, the axial lone pair leads to a higher energy transition state due to unfavorable steric interactions between the carbonyl and the axial hydrogens on the amine (Figure 4, **TS8**). For each orientation of the nitrogen lone pair, four piperidine conformations are available (Figure 6). In the most stable transition state (Figure 5 and Figure 6, **TS4**), the methyl group is on C2 of the piperidine and axial. The analogous equatorial conformation is slightly higher in energy (Figure 5, **TS1**). Location of the methyl group to the C6 piperidine carbon is significantly higher in energy due to steric interactions with the propionate (Figure 6, **TS2** and **TS3**).

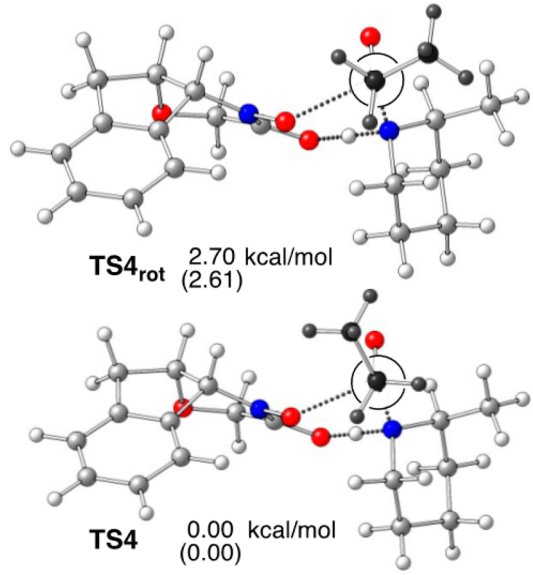

Figure 5. Newman projections of the transition state ethyl rotamers with relative solvated enthalpies (kcal/mol). Parenthetical values are the corresponding gas phase values.

A theoretical selectivity factor (Table 3) was calculated using the Boltzmann distribution from Table 2.[31] For both the ethyl and methyl substrates (entries 1 and 2), the model correctly anticipates that the (*S*)-enantiomer acylates more rapidly. In addition, the model expects that higher acyl congeners, such as

dx.doi.org/10.1021/ja505784w | J. Am. Chem. Soc. 2014, 136, 11783−11791

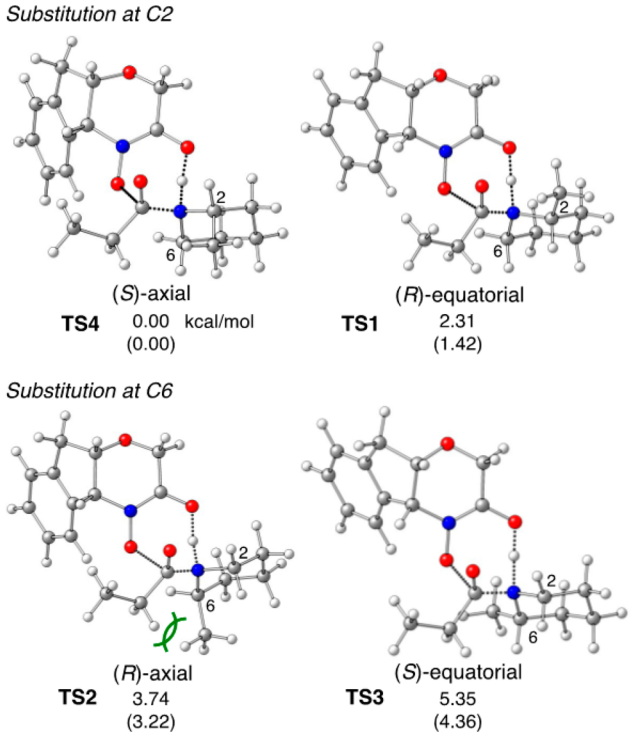

Figure 6. Four possible piperidine variations in the transition states with solvated relative enthalpies (kcal/mol). Parenthetical values are the corresponding gas phase values.

Table 3. Comparison of Experimental and Calculated Selectivity Factors (k_{rel} = S)

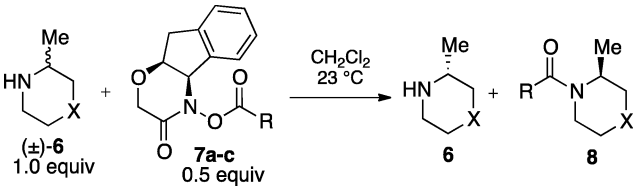

		selectivity factor (major amide product)		
entry	substrate	experiment[a]	calculated[c]	ΔG‡ of lowest energy transition state (kcal/mol)[d]
1	R = Et X = CH_2	14 (*S*)	12.79 (*S*)	22.0
2	R = Me X = CH_2	2 (*S*)	2.63 (*S*)	22.7
3	R = Et X = O	11(*S*)	10.6 (*S*)	24.3
4	R = Et X = S	NR[b]	12.5 (*S*)	25.7

[a]Experimental value employs R = *n*-butyl for entries 1 and 2, R = Bn for entries 3 and 4. [b]No reaction observed. [c]From IEFPCM-CH_2Cl_2-M06-2X/6-311+G(d,p)//B3LYP/6-31G(d,p) enthalpies at 25 °C. [d]IEFPCM-CH_2Cl_2-M06-2X/6-311+G(d,p)//B3LYP/6-31G(d,p)at 25 °C.

the propionyl, are more selective than the acetyl (calc k_{rel} = 12.79 vs 2.63) in accord with the experimental results (expt k_{rel} = 14 vs 2). Notably, one key transition state (**TS34**) accounts for most of the selectivity difference between the acetyl and propionyl cases. A steric interaction between the axial methyl group of the amine and the propionyl in **TS34** is absent in the acetyl analogue due to the shorter alkyl chain. Rotating the propionyl ethyl group to avoid this interaction in **TS34** only introduces other disfavorable steric interactions with the arene of the indane. The computed and experimental results are also in good agreement for the morpholine congener of the substrate (entry 3). Finally, the model predicts higher barriers for thiomorpholine in accord with the very low observed reactivity of this substrate (entry 4).

The structural differences between the lowest energy transition states leading to the acylated (*S*)-amine and the unreacted (*R*)-amine (Figure 4, **TS4** and **TS18**, respectively) suggest that increasing the penalty for the ethyl−indane interaction may serve to improve the selectivity. However, completely eliminating this pathway (Figure 4, **TS18**) will not give rise to a completely selective process due to other low-lying transition states from the enantiomeric starting material that are unaffected by this substituent, such as the (*R*)-equatorial transition state (Figure 6, **TS1**). Therefore, the design of improved catalysts requires taking into account multiple reaction pathways.

CONCLUSIONS

Our studies support a kinetic resolution of 2-alkyl cyclic amines via a concerted, seven-membered transition state involving a hydroxamic acid proton transfer. The energy of activation for this concerted pathway is 10.97 kcal/mol lower in energy than the next lowest pathway, which involves water catalysis. This study highlights the advantages of acyl transfer catalysts that also incorporate a group to enable proton transfer from the incoming nucleophile. Concerted amidation of the resultant activated esters via cyclic transition states is found to account for the relative reactivity of different peptide bond forming reagents, including HOAt and HOBt. This understanding can facilitate the development of further reagents for amide formation. The developed transition state models also accurately predict the products of the kinetic resolution reaction, suggesting that this model can be used for the logical de novo design of new catalysts for this substrate as well as for substrates that do not perform well using the current system.

EXPERIMENTAL SECTION

Calculation Methods. To identify the different reaction mechanisms, a conformational search was conducted for each transition state using the OPLS_2005 force field[38] as employed in MacroModel.[39] The lowest energy conformation was optimized at B3LYP/6-31G(d,p),[40,41] followed by single point calculations with implicit solvation (dichloromethane, ε = 8.93)[52] at IEFPCM-M06-2X/6-311+G(d,p)[42,43] using Gaussian09.[44] All DFT calculations employed an ultrafine integration grid (99 radial shells, 590 angular points) and tight optimization parameters. Frequency calculations confirmed the identity of geometry minima (no imaginary frequencies) and transition states (one imaginary frequency). Intrinsic reaction coordinate (IRC) calculations were performed to confirm the identity of identified transition states.[45] Local minima were found by nudging transition states along the reaction coordinate followed by geometry optimization and single point calculation at the levels described above. Gibbs free energies are given relative to starting materials at infinite distance; prereaction complexes were not considered. Zero-point enegies and thermal corrections were calculated at 298 K and are unscaled.

Transition state conformations to calculate selectivity factors were identified via systematic examination of variables rather than a Monte Carlo conformational search. All transition states were confirmed to have one imaginary frequency. Gas phase transition state geometry optimization was performed using B3LYP/6-31G(d,p) followed by

dx.doi.org/10.1021/ja505784w | J. Am. Chem. Soc. 2014, 136, 11783−11791

solvated single point energy calculations using M06-2X/6-311+G(d,p) and the IEFPCM solvation model (dichloromethane, ε = 8.93).

■ ASSOCIATED CONTENT

Supporting Information

Full computational and experimental details. This material is available free of charge via the Internet at http://pubs.acs.org.

■ AUTHOR INFORMATION

Corresponding Authors

marisa@sas.upenn.edu
bode@org.chem.ethz.ch

Notes

The authors declare no competing financial interest.

■ ACKNOWLEDGMENTS

We thank Michael Binanzer (ETH-Zürich) for preliminary kinetic studies. We are grateful to the National Institutes of Health (GM-079339 and GM-087605), the National Science Foundation (CHE-0449587), and the (ERC Starting Grant No. 306793-CASAA) for financial support of this research. Computational support was provided by XSEDE on SDSC Gordon (TG-CHE120052) and PSC Blacklight (TG-CHE110080). Additional computational support was provided by the NSF CRIF program, Grant CHE-013112, and the ETH High-Performance Cluster, Brutus.

■ REFERENCES

(1) Walsh, P. W.; Kozlowski, M. C. *Fundamentals of Asymmetric Catalysis*; University Science Books: Sausalito, CA, 2009.

(2) (a) Müller, C. E.; Schreiner, P. R. *Angew. Chem., Int. Ed.* **2011**, *50*, 6012. (b) Wende, R. C.; Schreiner, P. R. *Green Chem.* **2012**, *14*, 1821. (c) Krasnov, V. P.; Gruzdev, D. A.; Levit, G. L. *Eur. J. Org. Chem.* **2012**, 1471.

(3) Larionov, E.; Mahesh, M.; Spivey, A. C.; Wei, Y.; Zipse, H. *J. Am. Chem. Soc.* **2012**, *134*, 9390.

(4) Li, X.; Liu, P.; Houk, K. N.; Birman, V. B. *J. Am. Chem. Soc.* **2008**, *130*, 13836.

(5) Shinisha, C. B.; Sunoj, R. B. *Org. Lett.* **2009**, *11*, 3242.

(6) Sanan, T.; RajanBabu, T. V.; Hadad, C. M. *J. Org. Chem.* **2010**, *75*, 2369.

(7) Yang, X.; Bumbu, V. D.; Liu, P.; Li, X.; Jiang, H.; Uffman, E. W.; Guo, L.; Zhang, W.; Jiang, X.; Houk, K. N.; Birman, V. B. *J. Am. Chem. Soc.* **2012**, *134*, 17605.

(8) (a) Binanzer, M.; Hsieh, S.-Y.; Bode, J. W. *J. Am. Chem. Soc.* **2011**, *133*, 19698. (b) Hsieh, S.-Y.; Binanzer, M.; Kreituss, I.; Bode, J. W. *Chem. Commun.* **2012**, *48*, 8892−8894. (c) Kreituss, I.; Murakami, Y.; Binanzer, M.; Bode, J. W. *Angew. Chem., Int. Ed.* **2012**, *51*, 10660.

(9) For a subsequent report of an enzymetic resolution of N-heterocycles, see: Ghisleri, D.; Green, A. P.; Pontini, M.; Willies, S. C.; Rowles, I.; Frank, A.; Gorgan, G.; Turner, N. J. *J. Am. Chem. Soc.* **2013**, *135*, 10863.

(10) The reaction halts at 50% conversion with the use of 0.5 equiv hydroxamic ester.

(11) Sorrell, T. N. *Organic Chemistry*, 2nd Ed.; University Science Books: Sausolito, CA, 2006.

(12) (a) Sung, D. D.; Koo, I. S.; Yang, K.; Lee, I. *Chem. Phys. Lett.* **2006**, *426*, 280. (b) Singleton, D. A.; Merrigan, S. R. *J. Am. Chem. Soc.* **2000**, *122*, 11035.

(13) Satterthwait, A. C.; Jencks, W. P. *J. Am. Chem. Soc.* **1974**, *96*, 7018.

(14) Liu, X.-Q.; Jin, L.; Kim, C. K.; Xue, Y. *J. Mol. Catal. A.: Chem.* **2012**, *355*, 102.

(15) Hedstrom, L. *Chem. Rev.* **2002**, *102*, 4501.

(16) Oie, T.; Loew, G. H.; Burt, S. K.; Binkley, J. S.; MacElroy, R. D. *J. Am. Chem. Soc.* **1982**, *104*, 6169.

(17) Antonczak, S.; Ruiz-Lopez, M. F.; Rivail, J. L. *J. Am. Chem. Soc.* **1994**, *116*, 3912.

(18) (a) Yang, W.; Drueckhammer, D. G. *Org. Lett.* **2000**, *2*, 4133. (b) Yang, W.; Drueckhammer, D. G. *J. Am. Chem. Soc.* **2001**, *123*, 11004.

(19) Wang, L.-h.; Zipse, H. *Liebigs Ann. Chem.* **1996**, 1501.

(20) Gandour, R. D. *Tetrahedron Lett.* **1974**, *15*, 295.

(21) Duan, X.; Schreiner, S. *J. Am. Chem. Soc.* **1992**, *114*, 5849.

(22) (a) Rangelov, M. A.; Petrova, G. P.; Yomtova, V. M.; Vayssilov, G. N. *J. Org. Chem.* **2010**, *75*, 6782. (b) Rangelov, M. A.; Petrova, G. P.; Yomtova, V. M.; Vayssilov, G. N. *J. Mol. Graphics Modell.* **2010**, *29*, 246.

(23) Rangelov, M. A.; Vayssilov, G. N.; Yomtova, V. M.; D, P. D. *Org. Biomol. Chem.* **2005**, *3*, 737.

(24) Bunnett, J. F.; Davis, G. T. *J. Am. Chem. Soc.* **1960**, *82*, 665.

(25) (a) Ilieva, S.; Galabov, B.; Musaev, D. G.; Morokuma, K.; Schaefer, H. F. I. *J. Org. Chem.* **2003**, *68*, 1496. (b) Ilieva, S.; Atanasov, Y.; Kalcheva, V.; Galabov, B. *J. Mol. Struct.: THEOCHEM* **2003**, *633*, 49. (c) Galabov, B.; Atanasov, Y.; Ilieva, S.; Schaefer, H. F. I. *J. Phys. Chem. A* **2005**, *109*, 11470. (d) Galabov, B.; Ilieva, S.; Hadjieva, B.; Atanasov, Y.; Schaefer, H. F. I. *J. Phys. Chem. A* **2008**, *112*, 6700.

(26) Díaz, N.; Suárez, D.; Sordo, T. L.; Méndez, R.; Villacorta, J. M. *Eur. J. Org. Chem.* **2003**, 4161.

(27) Xia, X.; Zhang, C.; Xue, Y.; Kim, C. K.; Yan, G. *J. Chem. Theory Comput.* **2008**, *4*, 1643.

(28) (a) Rony, P. R. *J. Am. Chem. Soc.* **1969**, *91*, 6090. (b) Fischer, C. B.; Steininger, H.; Stephenson, D. S.; Zipse, H. *J. Phys. Org. Chem.* **2005**, *18*, 901.

(29) Petrova, T.; Okovytyy, S.; Gorb, L.; Leszczynski, J. *J. Phys. Chem. A* **2008**, *112*, 5224.

(30) Jin, L.; Wu, Y.; Kim, C. K.; Xue, Y. *J. Mol. Struct.: THEOCHEM* **2010**, *942*, 137.

(31) See Supporting Information for details.

(32) M06-2X/6-311+G(d,p) solvated single point calculations using B3LYP geometries are more effective than B3LYP alone in estimating absolute reaction barriers, see: Krenske, E. H.; Agopcan, S.; Aviyente, V.; Houk, K. N.; Johnson, B. A.; Holmes, A. B. *J. Am. Chem. Soc.* **2012**, *134*, 12010.

(33) Carpino, L. A. *J. Am. Chem. Soc.* **1993**, *115*, 4397.

(34) Carpino, L. A.; Imazumi, H.; Foxman, B. M.; Vela, M. J.; Henklein, P.; El-Faham, A.; Klose, J.; Bienert, M. *Org. Lett.* **2000**, *2*, 2253.

(35) The selectivity factor was calculated using enthalpy because the overall entropies of all the transition states are similar and enthalpies are known to be less prone to error than free energies: Cheong, P. H.-Y.; Legault, C. Y.; Um, J. M.; Çelebi-Ölçüm, N.; Houk, K. N. *Chem. Rev.* **2011**, *111*, 5042.

(36) Anet, F. A. L.; Yavari, I. *J. Am. Chem. Soc.* **1977**, *99*, 2794−2796.

(37) Erdogdu, Y.; Güllüoğlu, M. T. *Spectrochim. Acta, Part A* **2009**, *74*, 162.

(38) Kaminski, G. A.; Friesner, R. A.; Tirado-Rives, J.; Jorgensen, W. L. *J. Phys. Chem. B* **2001**, *105*, 6474.

(39) *MacroModel*, version 9.9; Schrödinger, LLC, New York, NY, 2012.

(40) (a) Becke, A. D. *J. Chem. Phys.* **1993**, *98*, 5648. (b) Lee, C.; Yang, W.; Parr, R. G. *Phys. Rev. B* **1988**, *37*, 785. (c) Vosko, S. H.; Wilk, L.; Nusair, M. *Can. J. Phys.* **1980**, *58*, 1200.

(41) (a) Ditchfield, R.; Hehre, W. J.; Pople, J. A. *J. Chem. Phys.* **1971**, *54*, 724. (b) Frisch, M. J.; Pople, J. A.; Binkley, J. S. *J. Chem. Phys.* **1984**, *80*, 3265.

(42) Cancès, E.; Mennucci, B.; Tomasi, J. *J. Chem. Phys.* **1997**, *107*, 3032.

(43) Zhao, Y.; Truhlar, D. G. *Theor. Chem. Acc.* **2008**, *120*, 215.

(44) Frisch, M. J.; Trucks, G. W.; Schlegel, H. B.; Scuseria, G. E.; Robb, M. A.; Cheeseman, J. R.; Scalmani, G.; Barone, V.; Mennucci, B.; Petersson, G. A.; Nakatsuj, H.; Caricato, M.; Li, X.; Hratchian, H. P.; Izmaylov, A. F.; Bloino, J.; Zheng, G.; Sonnenberg, J. L.; Hada, M.; Ehara, M.; Toyota, K.; Fukuda, R.; Hasegawa, J.; Ishida, M.; Nakajima, T.; Honda, Y.; Kitao, O.; Nakai, H.; Vreven, T.; J. A. Montgomery, J.;

Peralta, J. E.; Ogliaro, F.; Bearpark, M.; Heyd, J. J.; Brothers, E.; Kudin, K. N.; Staroverov, V. N.; Kobayashi, R.; Normand, J.; Raghavachari, K.; Rendell, A.; Burant, J. C.; Iyengar, S. S.; Tomasi, J.; Cossi, M.; Rega, N.; Millam, J. M.; Klene, M.; Knox, J. E.; Cross, J. B.; Bakken, V.; Adamo, C.; Jaramillo, J.; Gomperts, R.; Stratmann, R. E.; Yazyev, O.; Austin, A. J.; Cammi, R.; Pomelli, C.; Ochterski, J. W.; Martin, R. L.; Morokuma, K.; Zakrzewski, V. G.; Voth, G. A.; Salvador, P.; Dannenberg, J. J.; Dapprich, S.; Daniels, A. D.; Farkas, Ö.; Foresman, J. B.; Ortiz, J. V.; Cioslowski, J.; Fox, D. J. *Gaussian 09*, Revision C.01; Gaussian, Inc.: Wallingford, CT, 2009.

(45) Fukui, K. *Acc. Chem. Res.* **1981**, *14*, 363.